UDK 669.14.018.8:621.791 ISSN 1580-2949
Original scientific article/Izvirni znanstveni članek MTAEC9, 57(5)485(2023)

# OPTIMIZATION OF PROCESS PARAMETERS FOR A SOLID-STATE-WELDED AISI 430 STEEL JOINT WITH THE GRG REINFORCED RESPONSE SURFACE METHODOLOGY

## OPTIMIZACIJA PROCESNIH PARAMETROV TORNEGA VARJENJA JEKLA VRSTE AISI 430 Z GRG METODOLOGIJO OJAČANEGA ODGOVORA POVRŠINE

**G. Senthilkumar[1*], V. Vinodkumar[2], T. Mayavan[1], G. Rathinasabapathi[1], Amos Gamaleal David[1]**

[1]Department of Mechanical Engineering, Panimalar Engineering College, Chennai, Tamilnadu, India
[2]Department of Mechanical Engineering, Chennai Institute of Technology and Applied Research, Chennai, Tamilnadu, India

*Prejem rokopisa – received: 2023-05-04; sprejem za objavo – accepted for publication: 2023-07-28*

doi:10.17222/mit.2023.873

High-temperature applications such as heat exchangers and burner tubes employ AISI 430 steel. A larger heat-affected zone, undesired metallurgical changes and higher hardness in the weld area occur when fusion welding this type of steel. The study investigates the feasibility of welding ferritic stainless steel AISI 430, utilizing a solid-state method (continuous drive friction welding). The experiment uses an L27 orthogonal array and three levels of variation in the welding parameters such as frictional pressure, forging pressure, friction time, forging time and rotational speed. Tensile strength, axial shortening and impact toughness are the observed quality characteristics. In an integrated approach of the grey incidence reinforced response surface methodology, the benefits of the grey relational theory are merged with the statistical analysis of the response surface methodology to determine the ideal friction welding inputs (frictional pressure – 59.95 MPa, friction time – 4 s, upset pressure – 68.5 MPa, forging time – 3 s and rotational speed – 1399 $min^{-1}$). The AISI 430 steel joint's qualities are improved by 2.25, 12.74 and 7.89 % in terms of the maximum ultimate tensile strength, axial shortening and impact toughness, respectively.

Keywords: friction welding, optimization, response surface methodology, microstructure

Za visokotemperaturne aplikacije kot so toplotni izmenjevalniki in cevi gorilcev se uporablja feritno nerjavno jeklo vrste AISI 430. Večja toplotno vplivana cona, neželjene metalurške spremembe in višje trdote v področju zvarov so rezultat konvencionalega varjenja te vrste jekla, zaradi visokih temperatur in prisotnosti taline. Avtorji v tem članku opisujejo študijo izvedljivosti varjenja feritnega nerjavnega jekla vrste AISI 430 z metodo varjenja v trdnem stanju (kontinuirno varjenje s trenjem in mešanjem oziroma gnetenjem). Za preizkuse so izbrali ortogonalno matrico tipa L27 in tri nivoje variacij parametrov varjenja in sicer: tlak kovanja, čas trenja in hitrost vrtenja. Izbrani kriteriji kvalitete izdelanih zvarov so bili njihova natezna trdnost, osno skrajšanje in udarna žilavost. Z integriranim pristopom pojava v "sivem" z uporabo metodologije ojačanega odgovora površine so avtorji uporabili prednosti te metodologije oz. teorije v sivini (megli) in z znanjem na področju statistične analize RSM (angl.: Response Surface Methodology) določili idealne vhodne parametre varjenja (trenjski tlak – 59,95 MPa, čas trenja – 4 s, začetni tlak – 68,5 MPa, čas gnetenja – 3 s in hitrost vrtenja – 1399 $min^{-1}$). Kakovost zvarov jekla AISI 430 so na ta način izboljšali in sicer njihovo končno natezno trdnost za 2,25 %, aksialno skrajšanje za 12,74 % in udarno žilavost za 7,89 %.

Ključne besede: torno varjenje, optimizcija, metodologija odgovora površine, mikrostruktura.

## 1 INTRODUCTION

Pressure vessels and boilers are two common uses for the AISI 430 steel. The predominant choice for tubes and pipes in heat exchangers that carry hot fluids is AISI 430 steel due to its excellent tensile strength and impact toughness. The use of traditional liquid-state joining techniques to join AISI 430 steel raises several issues. A greater heat affected zone (HAZ) and the resulting changes in the parent metal's metallurgy occur with fusion welding processes. Liquid-state welding leads to microscopic corrosion along grain boundaries. This might have an impact on the joint's mechanical characteristics, which matter in applications involving high temperatures and stresses. Thus, joining AISI 430 steel in the solid state may increase the likelihood that such undesirable mechanical and metallurgical changes are minimized.

Since the temperature required for solid-state processing is far lower than the parent material's melting point, there is little to no HAZ produced. At the joint interface, the plastic flow of the material is seen. To limit the quantity of flash produced, the process governing the plastic flow of material at the weld contact is crucial. To lessen axial shortening, a reasonably lower flash is always preferred.[1] Observations of United Launch Alliance, Inc., detail crucial hardware advancements used to make joints in the solid state.[2] The mechanical properties of joints were shown to be considerably influenced by the friction welding inputs, including frictional pressure, upset pressure, burn-off length and rotational speed.[3] Grey relational analysis was used to optimize the param-

*Corresponding author's e-mail:
senthilngt1978@gmail.com (G. Senthilkumar)

eters of a typical TIG welding method used to join nuclear grade austenitic stainless steel 321. This improved the mechanical properties of the weld joints.[4] It was discovered that the temperature rise played a significant role in changing the qualitative characteristics of the bonds in the joints made between AISI 1050 and AISI 4140 steel. It was also discovered that the initial temperature increase was the highest, followed by a constant rise with continuous rotation, and the joints had no empty gaps.[5] The unaffected zone, moderately deformed zone and fully deformed zone are typically present at a solid-state friction welded interface. The fully distorted and moderately deformed zones show the most microstructural alterations.[6] By choosing the right values for the friction duration and rotational speed, a nearly flawless bonding strength that is close to that of the parent material can be achieved. The welding parameters have the biggest impact on how hot a friction interface becomes.[7] Due to the development of precipitates, friction-welded joints of high-strength nickel alloys show a tougher and stronger weld zone.[8]

It was discovered that the distribution of temperature and the plastic flow of material at the weld contact area is influenced by the rotational speed and frictional pressure.[9] For Al 6061 and an austenitic stainless steel joint, there is an increase in the efficiency of the friction-welded joint with a little increase in the frictional contact duration and a considerable increase in the upset pressure.[10] The friction-welded joint of AISI 304 with Al 6063 may have the best elbow bend ductility due to the high forging pressure.[11] Multi-objective friction welding of EN 10028 P 355 GH steel results in respectable amounts of tensile strength improvement and material savings.[12] The central composite design method for friction-welded ASTM A516 steel grade 70 leads to improvements in the tensile strength, impact toughness and reduced axial shrinkage.[13] Even without a model for the process, the genetic algorithm is a useful tool for experimental welding optimization; however, it is challenging to establish its parameters, such as population size and the number of generations for adequate sweeping of the search space. Though it suffers in an erratic experimental zone, the RSM technique was found to achieve a better compromise between evaluated results.[14] RSM is used to optimize the friction welding inputs for connecting UNS S32205 steel parts. For an experiment, the central composite design (CCD) was employed. To maximize the hardness and tensile strength, the upset pressure, friction pressure and speed of rotation were found to be the three most important parameters.[15] For the optimization of process parameters and modeling of the response values of diverse processes, hybrid approaches were applied. The advantages of the algorithms can now be combined benefits to these integrated techniques. The RSM approach and grey relational analysis are used for response modeling and optimization.[16] Being a statistical tool for optimization, the method is used to produce response surfaces to investigate how different design variables interact with one another. The two most popular response surface designs are typically the central composite design and the Box-Behnken design[17].

The TIG welding procedure was used to join a Fe-2.25Cr-1Mo steel tube with a carbon steel tube while employing a filler material that contained chromium. The weld's corrosion resistance behavior was enhanced by the production of $Cr_2O_3$ caused by the presence of chromium.[18] A forged low-alloy steel tube and a drawn low-alloy steel tube are successfully joined by solid-state friction welding and the input parameters are optimized with the response surface methodology to enhance the required properties.[19] A surge in the friction force increases the heat generation at the interface and tends to make better bonding of the material, leading to a high tensile strength.[20] The carbide-free interface obtained with the friction welding of A516 steel and 316L steel shows no sensitization during the process.[21] The load-carrying ability of an asymmetric friction-welded joint depends upon the grain size in the microstructure.[22]

Even though AISI 430 steel has significant applications in heat exchanger tubes, there is not enough information in the literature about the solid-state joining of this material. Furthermore, scientific literature pays little attention to designing welding parameters for AISI 430 steel. In order to provide instructions and a welding database for joining AISI 430 steel with the friction welding technique, this work investigates the feasibility of generating high-quality welded connections utilizing continuous drive friction welding. Although orthogonal arrays-based RSM is used in some manufacturing processes, there is little information about it in the literature. Thus, by using a hybrid approach of the grey relational analysis and reinforced response surface methodology for the optimal parameter design, the potential for simultaneous optimization of numerous responses is increased in the proposed work.

## 2 MATERIALS AND METHODS

The AISI 430 steel used for heat exchanger tubes was procured in the form of a rod with a diameter of 16 mm. The chemical composition and material properties of the parent material are listed in **Tables 1** and **2**, respectively.

**Table 1:** Composition of AISI 430 steel by maximum weight

| Element | C | Mn | Si | Cr | P | Mo | Ni | Fe |
|---|---|---|---|---|---|---|---|---|
| % | 0.13 | 1.58 | 0.41 | 16.38 | 0.038 | 0.21 | 0.46 | Remaining |

**Table 2:** Material properties of AISI 430 steel

| S. No. | Properties | Value | Unit |
|---|---|---|---|
| 1 | Yield strength | 410 | $N/mm^2$ |
| 2 | Ultimate tensile strength | 555 | $N/mm^2$ |
| 3 | Impact toughness | 28 | J |

The friction welding of rods, cut to a length of 130 mm each, was done in a friction welding machine made by RV Machine Tools in Coimbatore, India.

The device has a hydraulic chuck with a spindle set to 12 kW and a maximum speed of 3000 min$^{-1}$. The friction welding settings are accurately set by "Indra Control VCP-02" at the operator terminal, and the slide is driven by a servomotor gearbox.

The machine contains a built-in "Rexroth controller" component made by Bosch Rexroth's automated assembly section in Germany. A smooth transition between various stages of a joint development is ensured with the necessary parameter setup. **Figures 1** and **2** show the beginning of the friction welding process, the upset that occurs, and the development of flash at the weld contact. Preliminary experiments were used to determine the values of different parameters, resulting in bonds with no visible flaws or failures. Based on the prior instructions from scientific literature, trials were carried out to determine the ranges of various parameters. The levels of various welding parameters employed in experimentation are shown in **Table 3**.

During friction welding, Rexroth spindle drive was used to accurately control one half of the joint while holding the other half motionless and ready to slide. After verifying that both of the components to be joined had an equal amount of overhang, they were then permitted to come into contact. A smooth transition between various stages of the joint development was ensured with the necessary parameter setup. The tests were carried out using Taguchi's orthogonal array ($L_{27}$), which made it possible to investigate the essential interactions between different design variables. Axial shortening (AS), impact toughness (IT) and ultimate tensile strength (UTS) were the quality attributes. The experiments were carried out at random to lessen the influence of uncontrollable circumstances, and the created joints were examined for quality attributes. The sample joints formed are shown in **Figure 3**. After preparing a specimen in accordance with ASTM E8, a tension test was carried out in an Instron computerized tension tester. The reduction in the length of the final joint obtained with friction welding was identified as axial shortening. An indicator of the toughness of a sample is the amount of energy absorbed by the specimen during fracture as seen during the impact test.

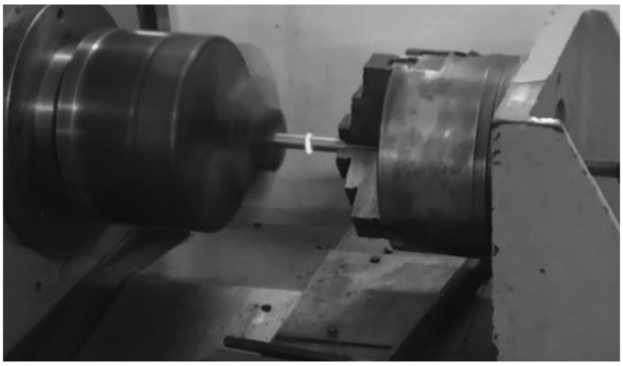

**Figure 1:** Application of friction pressure in the initial phase

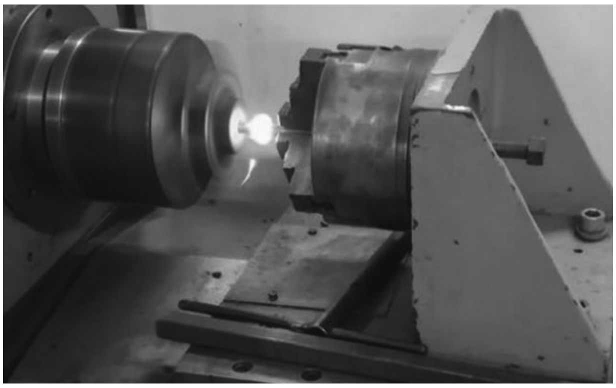

**Figure 2:** Upset and flash formation

**Table 3:** Levels of various friction-welding inputs

| Input parameters | Unit | Symbol | Levels | | |
|---|---|---|---|---|---|
| | | | Level 1 | Level 2 | Level 3 |
| Friction pressure (FP) | N/mm$^2$ | A | 40 | 50 | 60 |
| Upset pressure (UP) | N/mm$^2$ | B | 50 | 60 | 70 |
| Friction time (FT) | s | C | 3 | 5 | 7 |
| Upset time (UT) | s | D | 3 | 5 | 7 |
| Speed | min$^{-1}$ | E | 1000 | 1200 | 1400 |

**Table 4:** Experimental results for friction welded AISI 430 steel joints

| Trial | Process parameters | | | | | Responses | | |
|---|---|---|---|---|---|---|---|---|
| | FP (MPa) | UP (MPa) | FT (s) | UT (s) | Speed (min$^{-1}$) | UTS (MPa) | AS (mm) | IT (J) |
| 1 | 40 | 50 | 3 | 3 | 1000 | 518 | 10.93 | 14 |
| 2 | 40 | 50 | 5 | 5 | 1200 | 514 | 10.88 | 16 |
| 3 | 40 | 50 | 7 | 7 | 1400 | 519 | 10.53 | 20 |
| 4 | 40 | 60 | 3 | 5 | 1400 | 508 | 5.75 | 18 |
| 5 | 40 | 60 | 5 | 7 | 1000 | 515 | 5.98 | 21 |
| 6 | 40 | 60 | 7 | 3 | 1200 | 507 | 6.30 | 18 |
| 7 | 40 | 70 | 3 | 7 | 1200 | 518 | 17.78 | 23 |
| 8 | 40 | 70 | 5 | 3 | 1400 | 517 | 17.20 | 15 |
| 9 | 40 | 70 | 7 | 5 | 1000 | 519 | 17.51 | 19 |
| 10 | 50 | 50 | 3 | 3 | 1000 | 507 | 35.51 | 16 |
| 11 | 50 | 50 | 5 | 5 | 1200 | 510 | 34.30 | 18 |
| 12 | 50 | 50 | 7 | 7 | 1400 | 515 | 33.87 | 19 |
| 13 | 50 | 60 | 3 | 5 | 1400 | 530 | 14.53 | 23 |
| 14 | 50 | 60 | 5 | 7 | 1000 | 523 | 12.67 | 15 |
| 15 | 50 | 60 | 7 | 3 | 1200 | 521 | 13.31 | 19 |
| 16 | 50 | 70 | 3 | 7 | 1200 | 523 | 16.65 | 16 |
| 17 | 50 | 70 | 5 | 3 | 1400 | 525 | 15.43 | 20 |
| 18 | 50 | 70 | 7 | 5 | 1000 | 521 | 16.12 | 18 |
| 19 | 60 | 50 | 3 | 3 | 1000 | 507 | 17.78 | 18 |
| 20 | 60 | 50 | 5 | 5 | 1200 | 510 | 17.58 | 23 |
| 21 | 60 | 50 | 7 | 7 | 1400 | 514 | 17.60 | 15 |
| 22 | 60 | 60 | 3 | 5 | 1400 | 523 | 18.08 | 20 |
| 23 | 60 | 60 | 5 | 7 | 1000 | 521 | 17.95 | 18 |
| 24 | 60 | 60 | 7 | 3 | 1200 | 532 | 18.68 | 19 |
| 25 | 60 | 70 | 3 | 7 | 1200 | 534 | 8.89 | 18 |
| 26 | 60 | 70 | 5 | 3 | 1400 | 532 | 18.68 | 19 |
| 27 | 60 | 70 | 7 | 5 | 1000 | 536 | 9.53 | 15 |

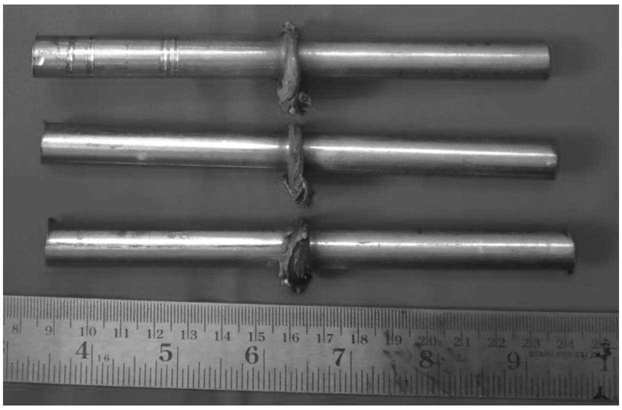

**Figure 3:** Samples of friction welded joints

This provides the opportunity for additional research on the ductile-brittle transition. According to the ASTM E23 standard, Charpy V-notch testing (the pendulum type) was done. The experimental results obtained are shown in **Table 4**.

## 3 GREY RELATIONAL GRADE REINFORCED RESPONSE SURFACE METHODOLOGY

The RSM is a statistical method featuring a module for modeling design variables and a desirability analysis module for enhancing the results. 3D surface graphs are used to demonstrate how parameters affect responses. The ability of the grey incidence analysis to handle uncertainty is combined with RSM modeling skills in the integrated strategy of the grey incidence reinforced response surface technique and the process parameters are optimized with the grey relational gradient reinforced response surface methodology.[12] The grey relational gradient is one of the methods for converting a multi-objective function into a single-objective function for the optimization of process parameters.[4] Previously several investigations had been tried to find the optimum conditions based on trials, but minimum literature is available on the optimization of friction welding parameters for maximizing the tensile strength. Multi-objective optimization, increasing the impact toughness and tensile strength, and reducing axial shrinkage of friction welded joints is almost non-existent. Therefore, in this work, multi-objective optimization for surging the impact toughness and tensile strength, and reducing axial shrinkage of friction welded joints was integrated with the grey relational gradient reinforced response surface methodology. The step-by-step procedure of the grey relational grade reinforced response surface methodology is as follows.

### *3.1 Stage 1: Grey relational grade (GRG) analysis*

In the first stage, the S/N ratio is calculated from the experimental data. The normalization of the S/N ratio converts experimental values from zero to one. The normalized data is further processed, being projected as the single quantity of various output responses obtained from experimentations.

**Step 1:** Calculation of the S/N ratio for each response using the exact equation based on its quality requirements. The larger-the-best type of quality characteristics is used for maximizing the tensile strength and impact toughness while the smaller-the-best type is used for minimizing the axial shortening. The S/N ratio ($\eta$) values for responses are obtained with Equations (3.1) and (3.2).

$$\textit{Larger-the-best}: \frac{S}{N}\,\text{ratio}(\eta) = -10\,\text{lg}\left(\frac{1}{n}\right)\sum_{i=1}^{n}\frac{1}{y_i^2} \tag{3.1}$$

$$\textit{Smaller-the-best}: \frac{S}{N}\,\text{ratio}(\eta) = -10\,\text{lg}\left(\frac{1}{n}\right)\sum_{i=1}^{n} y_i^2 \tag{3.2}$$

where $n$ = No. of replications, $y_i$ = observed output values, $i$ = 1,2,3… $n$.

**Step 2:** Normalized S/N ratio ($Z_i$) estimated using Equation (3.3)

$$Z_i = \frac{y_i - \min(y_i, i = 1,2,\ldots,n)}{\max(y_i, i = 1,2,\ldots,n) - \min(y_i, i = 1,2,\ldots,n)} \tag{3.3}$$

**Step 3:** Calculation of grey relational coefficient ($\gamma$) values using Equation (3.4)

$$y_i^j = \frac{\Delta\min + \xi\Delta\max}{\Delta_{oj}(i) + \xi\Delta\max} \tag{3.4}$$

$\Delta_{oj} = \left\| z_0(i) - z_j(i) \right\|$, $z_0(i)$ is the reference sequence $z_0(i)$ = 1; $I$ = 1, 2,…,$n$), $z_j(i)$ is the smallest value of $z_j(i)$, and '$\xi$' is the distinguishing coefficient $0 \leq \xi \leq 1$ which is taken as 0.5.

**Step 4:** Calculation of grey relational gradient (GRG) values ($\gamma_i$) for every trial using Equation (3.5)

$$GRG_i = \frac{1}{n}\sum_{i=1}^{n}(\gamma_i) \tag{3.5}$$

### *3.2 Stage II: Grey relational grade (GRG) reinforced RSM*

A single-quality measure representing various outputs in terms of GRG is obtained. This GRG value is utilized with the RSM technique to generate a second order model. The influences of input parameters are observed in the response surface plots.

**Step 5:** ANOVA with GRG values is used to determine the substantial contribution of process parameters.

**Step 6:** A second order model is developed to associate the GRG with the inputs and their interactions.

**Step 7:** The desirability analysis is used to find the optimum welding conditions. The influence of input parameters on the GRG is studied with the response surface plot. The optimized results are validated by the experimentation.

### *3.3 Grey incidence analysis and GRG values of friction welded ferritic stainless steel*

The S/N ratios and normalized values of S/N ratios for quality characteristics of the friction welded AISI 430 joints are presented in **Table 5**. The grey relational coefficient, GRC, grey relational gradient, GRG, and GRG values predicted from the developed model for all the trials are included in **Table 6**.

**Table 5:** S/N ratio and normalized S/N ratio for AISI 430 steel friction welded joints

| Trial | S/N ratio | | | Normalized S/N ratio | | |
|---|---|---|---|---|---|---|
| | UTS | AS | IT | UTS | AS | IT |
| 1 | 54.100 | -15.193 | 22.923 | 0.000 | 1.000 | 0.000 |
| 2 | 54.151 | -19.956 | 24.609 | 0.106 | 0.699 | 0.391 |
| 3 | 54.270 | -20.812 | 24.444 | 0.352 | 0.645 | 0.817 |
| 4 | 54.287 | -28.165 | 24.082 | 0.386 | 0.180 | 0.269 |
| 5 | 54.117 | -24.711 | 23.522 | 0.036 | 0.398 | 0.139 |
| 6 | 54.185 | -24.428 | 25.105 | 0.177 | 0.416 | 0.506 |
| 7 | 54.202 | -25.506 | 24.609 | 0.212 | 0.348 | 0.391 |
| 8 | 54.185 | -28.787 | 27.235 | 0.177 | 0.140 | 1.000 |
| 9 | 54.100 | -28.787 | 26.444 | 0.000 | 0.140 | 0.817 |
| 10 | 54.151 | -15.534 | 24.609 | 0.106 | 0.978 | 0.391 |
| 11 | 54.287 | -25.144 | 26.444 | 0.386 | 0.371 | 0.817 |
| 12 | 54.353 | -29.994 | 26.848 | 0.525 | 0.064 | 0.910 |
| 13 | 54.403 | -29.367 | 26.444 | 0.628 | 0.104 | 0.817 |
| 14 | 54.253 | -28.787 | 24.609 | 0.317 | 0.140 | 0.391 |
| 15 | 54.270 | -29.127 | 26.444 | 0.352 | 0.119 | 0.817 |
| 16 | 54.253 | -30.238 | 27.235 | 0.317 | 0.049 | 1.000 |
| 17 | 54.320 | -29.571 | 27.235 | 0.456 | 0.091 | 1.000 |
| 18 | 54.287 | -29.686 | 26.848 | 0.386 | 0.083 | 0.910 |
| 19 | 54.420 | -20.749 | 24.082 | 0.662 | 0.649 | 0.269 |
| 20 | 54.370 | -28.818 | 26.444 | 0.559 | 0.138 | 0.817 |
| 21 | 54.583 | -30.832 | 24.609 | 1.001 | 0.011 | 0.391 |
| 22 | 54.567 | -29.066 | 24.609 | 0.967 | 0.123 | 0.391 |
| 23 | 54.403 | -28.818 | 24.082 | 0.628 | 0.138 | 0.269 |
| 24 | 54.370 | -29.686 | 24.609 | 0.559 | 0.083 | 0.391 |
| 25 | 54.453 | -28.787 | 24.609 | 0.730 | 0.140 | 0.391 |
| 26 | 54.583 | -30.906 | 26.444 | 1.001 | 0.006 | 0.817 |
| 27 | 54.453 | -31.005 | 27.235 | 0.730 | 0.000 | 1.000 |

**Table 6:** Calculations of the GRG of the AISI 430 friction welded joints

| Trial | Grey relational coefficient (GRC) | | | Actual (GRG) | Predicted (GRG) |
|---|---|---|---|---|---|
| | UTS | AS | IT | | |
| 1 | 0.333 | 1.000 | 0.333 | 0.5556 | 0.5712 |
| 2 | 0.359 | 0.624 | 0.451 | 0.4779 | 0.4815 |
| 3 | 0.435 | 0.585 | 0.732 | 0.5839 | 0.5898 |
| 4 | 0.449 | 0.379 | 0.406 | 0.4113 | 0.4251 |
| 5 | 0.341 | 0.454 | 0.367 | 0.3875 | 0.3956 |
| 6 | 0.378 | 0.461 | 0.503 | 0.4474 | 0.4912 |
| 7 | 0.388 | 0.434 | 0.451 | 0.4243 | 0.4615 |
| 8 | 0.378 | 0.368 | 1.000 | 0.5818 | 0.5776 |
| 9 | 0.333 | 0.368 | 0.732 | 0.4776 | 0.4618 |
| 10 | 0.359 | 0.959 | 0.451 | 0.5894 | 0.5514 |
| 11 | 0.449 | 0.443 | 0.732 | 0.5411 | 0.5518 |
| 12 | 0.513 | 0.348 | 0.848 | 0.5696 | 0.5612 |
| 13 | 0.573 | 0.358 | 0.732 | 0.5543 | 0.5216 |
| 14 | 0.423 | 0.368 | 0.451 | 0.4137 | 0.4218 |
| 15 | 0.435 | 0.362 | 0.732 | 0.5097 | 0.4903 |
| 16 | 0.423 | 0.344 | 1.000 | 0.5889 | 0.5756 |
| 17 | 0.479 | 0.355 | 1.000 | 0.6111 | 0.6212 |
| 18 | 0.449 | 0.353 | 0.848 | 0.5500 | 0.5715 |
| 19 | 0.597 | 0.587 | 0.406 | 0.5300 | 0.5416 |
| 20 | 0.531 | 0.367 | 0.732 | 0.5434 | 0.5318 |
| 21 | 1.000 | 0.336 | 0.451 | 0.5960 | 0.5625 |
| 22 | 0.938 | 0.363 | 0.451 | 0.5840 | 0.5714 |
| 23 | 0.573 | 0.367 | 0.406 | 0.4488 | 0.4361 |
| 24 | 1.000 | 0.335 | 0.732 | 0.6892 | 0.6915 |
| 25 | 0.650 | 0.368 | 0.451 | 0.4894 | 0.4866 |
| 26 | 0.531 | 0.353 | 0.451 | 0.4451 | 0.4619 |
| 27 | 0.650 | 0.333 | 1.000 | 0.6609 | 0.6306 |

**Figure 4** shows the variations in the GRG values for the 27 experimental runs. The maximum value of the GRG was 0.6892 (24$^{th}$ trial), closely matching experimental conditions, being a near-optimal value.

## 4 RESULTS AND DISCUSSION

### *4.1 Quadratic model for the GRG (AISI 430 steel)*

The Design-Expert software was used to create a quadratic model for the GRG, i.e., Equation (4.1):

$$GRG = 3.5025 - 0.0116A - 0.0915B - 0.0566C - 0.0724D + 0.0001E + 0.0002AB + 0.0119CD + 0.0006B^2 \quad (4.1)$$

**Table 7** presents the ANOVA of the GRG reinforced RSM model for a friction welded AISI 430 steel joint. The F-value of 8.31 and p-value of 0.0001 attained for this second-order model show that this model is significant. A p-value of less than 0.05 indicates a significant importance of parameters (A, B, D and E) and their interactions (AB and CD). The second order of term A was also significant in influencing the GRG and hence the responses. The R-square value of 0.7869, the predicted R-square value of 0.5089, and the adjusted R-square value of 0.6921 are near to 1 showing this model is relevant. The adequate precision is 12.2354, which is greater than 4, thus signifying the sufficiency of the model. **Figure 5** shows the closeness of the actual and predicted

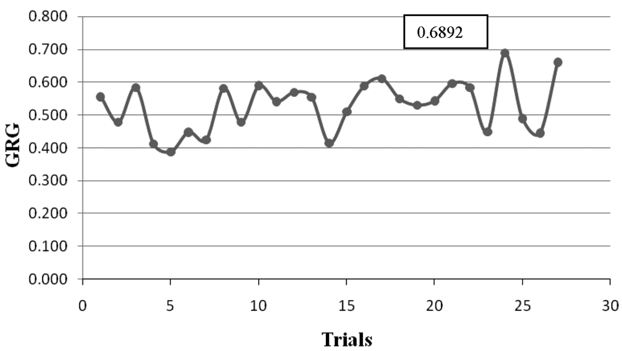


**Figure 4:** Graph of GRG values for $L_{27}$ OA experimental runs

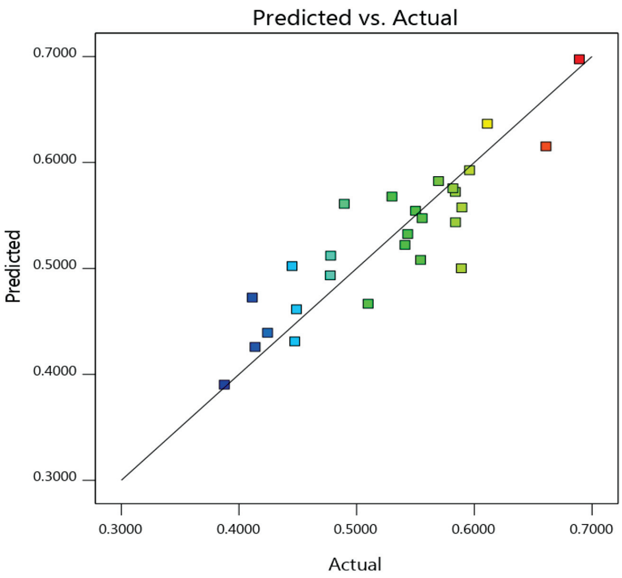


**Figure 5:** Plot of predicted versus actual GRG values

values of response (GRG) for the 27 trials. The predicted and actual GRG values are very close on the diagonal. This shows that the developed model is relevant.[12] **Figure 6** shows the graph of internally studentized residuals. The bulk residuals are positive or along the diagonal line, with a nearly symmetric distribution and no discernible trends. The fit of the produced model for the response is further determined by the randomness in the residual plot.

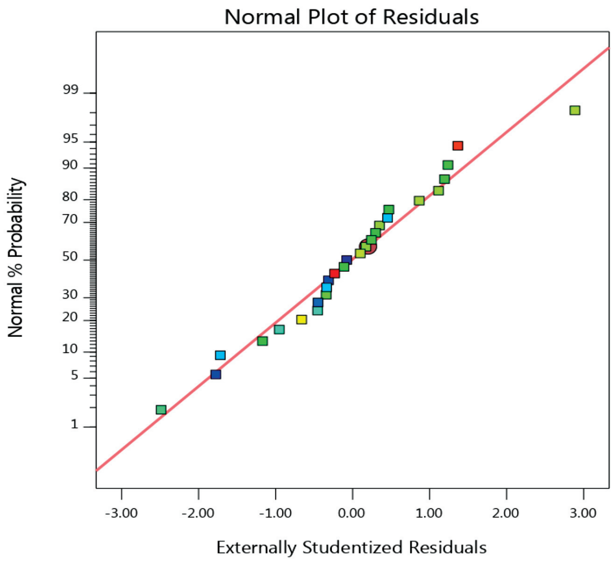


**Figure 6:** Graph of internally studentized residuals

**Table 7:** ANOVA for the response surface quadratic model for an AISI 430 FW joint

| Source | Sum of squares | DOF | Mean sum of square | F-value | p-value | Re-marks |
|---|---|---|---|---|---|---|
| Model | 0.1256 | 8 | 0.0157 | 8.31 | 0.0001 | Significant |
| A – Frictional pressure | 0.0215 | 1 | 0.0215 | 11.31 | 0.0049 | |
| B – Upset pressure | 0.0245 | 1 | 0.0245 | 12.89 | 0.0009 | |
| C – Friction time | 0.0007 | 1 | 0.0007 | 0.375 | 0.5477 | |
| D – Forging time | 0.0116 | 1 | 0.0116 | 6.15 | 0.0233 | |
| E – Rotational speed | 0.0129 | 1 | 0.0129 | 6.78 | 0.0065 | |
| AB | 0.0077 | 1 | 0.0077 | 4.07 | 0.0588 | |
| CD | 0.0137 | 1 | 0.0137 | 7.25 | 0.0149 | |
| $B^2$ | 0.0223 | 1 | 0.0223 | 11.79 | 0.0030 | |
| Residual | 0.0340 | 18 | 0.0019 | | | |
| Cor. total | 0.1596 | 26 | | | | |

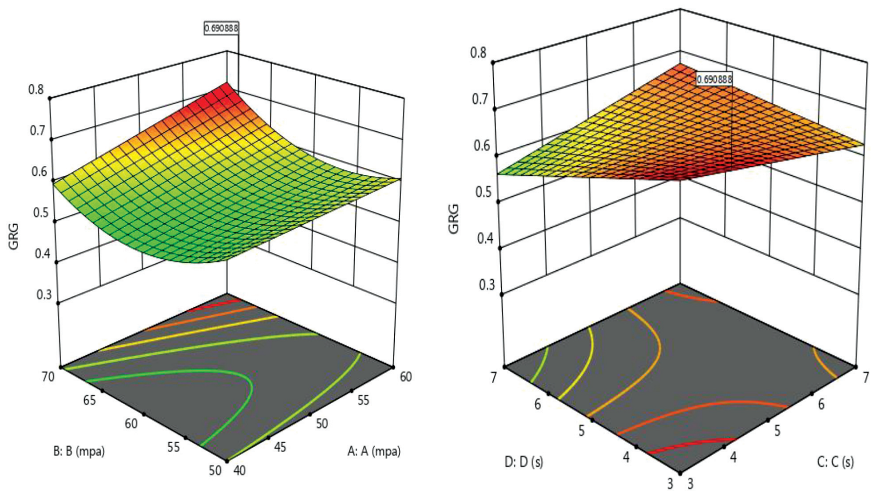


**Figure 7:** a) Effect of parameters on GRG A and B, b) Effect of parameters on GRG C and D

### *4.2 Analysis of response surface plots (AISI 430 steel)*

The response surface plots in **Figure 7a** show that a high value of frictional pressure of 59.95 MPa produces a better response. **Figure 7b** shows a low level of friction time of 4 seconds, which was sufficient to generate the temperature and heat at the interface. A larger value of upset pressure of 68.5 MPa allowed a larger GRG, which is shown in **Figure 7a** and hence, an improved response.

### *4.3 Ramp graph and desirability analysis of GRG values (AISI 430 steel)*

The desirability analysis is a method of finding a good set of conditions that meet all the goals. The point, at which the maximum desirability function gives the optimum operating conditions, is equal to one.[16] The optimal conditions were determined in terms of input parameters that produced the highest values of desirability (A – 59.95 MPa, B – 68.5 MPa, C – 4 s, D – 3 s and E – 1399 $min^{-1}$). The desirability analysis output is presented in **Table 8**. **Figure 8** shows the optimal levels of input parameters. The input parameters with the highest desirability are shown in the ramp graphs. The highest desirable levels of all input parameters in the range of permissible levels are marked as red dots, hence indicating that the highest value of GRG is 0.6908. This value lies between the 95 % confidence level lower limit of 0.6259 and the upper limit of 0.7556. This shows that the predicted optimum conditions have a chance of a 5 % error.

### *4.4 Confirmation test for a friction welded AISI 430 steel joint*

The outputs of the experimental trial No. 24 with the highest computed value of GRG (0.6892) were compared to the outputs anticipated by the grey incidence reinforced response surface approach with the optimal setup of the welding inputs. The quality attributes of the joint formed with optimal welding inputs were improved, proving the methodology used for the multi-response optimization was efficient. The joint properties including an ultimate tensile strength (UTS) of 544 MPa and impact toughness (IT) of 20.5 J are obtained under optimal conditions and the properties of the base metal are UTS = 555 MPa and IT = 28 J. The axial shortening of 16.3 mm obtained with the optimal setting of welding inputs was substantially remarkable. As a result, a good bond with good mechanical properties can be achieved using only modest shortening values.

The enhancement of the properties including the maximum ultimate tensile strength, impact toughness and axial shortening obtained for the AISI 430 steel joint is (2.25, 7.89 and 12.74) %, respectively. The increase in the forging pressure is the reason for the improvement in the strength and the decrease in the friction time is the reason for bringing down the axial shrinkage.[23] These details are listed in **Table 9**.

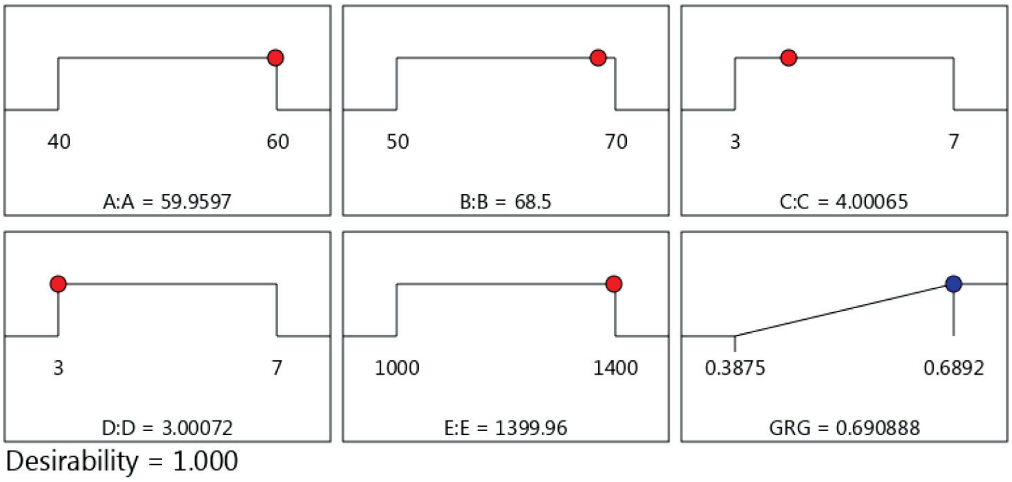


**Figure 8:** Ramp graphs with optimal levels of friction welding inputs

**Table 8:** Welding input parameters at optimal levels for AISI 430 steel

| Symbol | Welding inputs | Low level | High level | Optimum level |
|---|---|---|---|---|
| A | Friction pressure | 40 | 60 | 59.95 |
| B | Upset pressure | 50 | 70 | 68.5 |
| C | Frictional time | 3 | 7 | 4 |
| D | Forging time | 3 | 7 | 3 |
| E | Rotational speed | 1000 | 1400 | 1399 |
| Response | Prediction | SE mean | 95 % CI high | 95 % CI low |
| GRG | 0.69088 | 0.0308 | 0.7556 | 0.6259 |

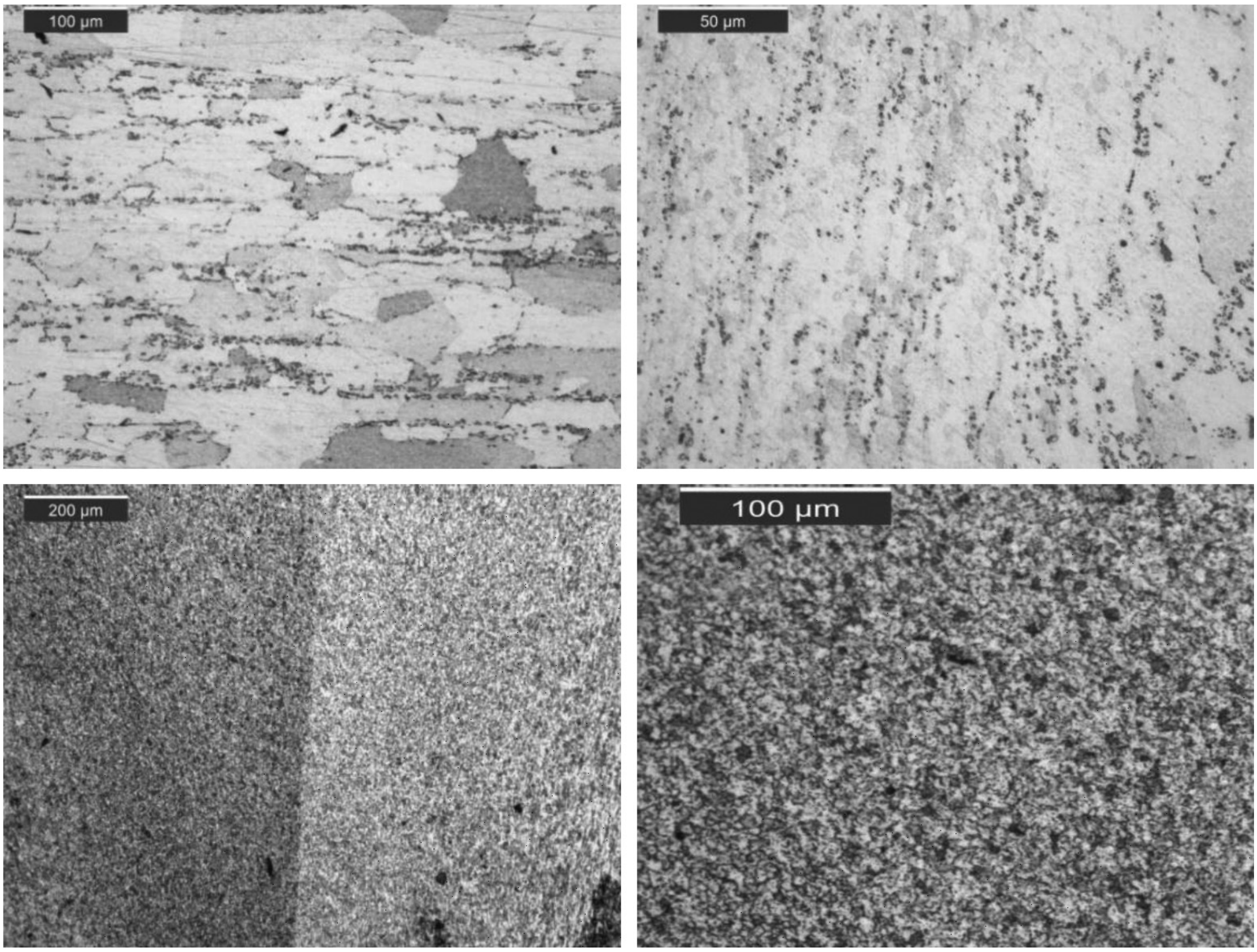


**Figure 9:** a) Unaffected zone, b) heat affected zone, c) weld interface, d) plastically deformed zone

**Table 9:** Comparison of the results for optimal setting of welding inputs

| Responses | Initial setting | Optimal set esetting | Enhance-ment | % En-hance-ment |
|---|---|---|---|---|
| GRG | 0.6892 | 0.6908 | 0.0016 | – |
| Ultimate Tensile Strength (MPa) | 532 | 544 | 12 | 2.25 |
| Axial Shortening (mm) | 18.68 | 16.30 | 2.38 | 12.74 |
| Impact Toughness (J) | 19 | 20.5 | 1.5 | 7.89 |

## 5 MACROSCOPIC AND MICROSCOPIC EXAMINATIONS

The thermal input required for the softening of material closer to the weld contact is produced by the heat flux as a result of the frictional pressure and rotational speed. Applying the right amount of upset pressure causes plastic flash, or radial outward displacement of the material closer to the interface. The weld penetration was fully accomplished because there was no longer any trace of the weld line, and the curl of the parent material was visible in the form of a flash. A closer look at the flash under a microscope reveals that it is consistent in breadth, demonstrating the strength of the bond. The heat generation of friction welding is completely different from the metal fusion welding technique, but the uniformity of the temperature distribution is observed from the weld interface to the unaffected zone. Various microstructures are identified between the weld interface and the base metal due to the temperature gradient.[24]

The microstructures of the unaffected zone, heat affected zone, weld interface and plastically deformed zone are shown in **Figures 9a** to **9d**, obtained with the optical microscope. The unaffected region shows that the plastic flow has stopped and the parent material is beginning to move away from the joint interface on both sides, as seen in **Figure 9a**.

The chromium carbides seen at the ferritic boundaries in the microstructure of the heat affected zone in **Figure 9b** show that chromium does not transform to austenite because of heating. Therefore, the weld interface in **Figure 9c** shows increased evidence of material softening caused by the thermal input. The remaining portion of the parent material is not impacted by the temperature or stress, minimizing the probability of unfavorable microstructural changes and property degradation in fusion welded joints.

The plastically deformed zone contains a finer grain structure, whereas the partially deformed zone contains a coarse grain structure as shown in **Figure 9d**. Due to faster rotating speeds, the microstructure at the weld contact exhibits dynamic recrystallization. Due to the high temperature, stress and distortion that it experienced, the weld interface seems to be considerably darker than the other regions. Due to the torque that the rotation experiences at higher temperatures, the grains appear to be dragged into the zone of moderate deformation. It was discovered that the advancing portion of the joint has more drag than the retreating portion.

## 6 CONCLUSIONS

A successful attempt to join AISI 430 steel pieces in the solid state was made, and the potential for creating high-quality welded joints utilizing continuous drive friction welding was investigated. Using the integrating strategy of the grey incidence incorporated response surface methodology for the optimal parameter selection, the potential for a concurrent optimization of numerous responses is increased. The usage of the $L_{27}$ orthogonal array in experimental trials, as opposed to more traditional approaches that used CCD or BBD, with the standard RSM to determine the ideal friction welding inputs resulted in a significant reduction in the number of experiments.

The maximum ultimate tensile strength, impact toughness and axial shortening for the highest GRG of friction welded AISI 430 steel are 532 MPa, 19 J and 18.68 mm, respectively. The maximum ultimate tensile strength, impact toughness and axial shortening obtained under optimum conditions are 544 MPa, 20.5 J and 16.3 mm, respectively. The improvement in the maximum ultimate tensile strength, impact toughness and axial shortening of the desired joint is (2.25, 7.89 and 12.74) %, respectively. Improvements of nearly 98 % for the ultimate tensile strength and 73.21 % for the impact toughness are achieved when compared to the parent material. In terms of linking various welding inputs and forecasting the outcomes in terms of grey relational grade, the created quadratic model was sufficient and efficient. It was discovered that the anticipated and experimentally observed values were rather close, proving the model's suitability. The quality characteristics of the joints were discovered to be influenced by both the individual welding settings and their interactions. The study can be extended further to modeling the temperature at a weld interface.

## Acknowledgment

The authors would like to extend their sincere gratitude for the facilities provided by the Panimalar Engineering College, Department of Mechanical Engineering, Chennai, India.

## 7 REFERENCES

[1] B. L. Benn, B. Towler, Control of Friction and Inertia Welding Processes, Patent No. US4757932A, 1988

[2] D. M. Potter, R. K. Hansen, Friction Welding Apparatus, System and Method, Patent No. US8123104B1, 2012

[3] S. T. Selvamani, M. Vigneshwar, K. Palanikumar, D. Jayaperumal, The corrosion behavior of fully deformed zone of friction welded low chromium plain carbon steel joints in optimized condition, J. Braz. Soc. Mech. Sci. Eng., 40 (**2018**), 305–317, doi:10.1007/s40430-018-1129-1

[4] S. Mohan Kumar, S. Sankarapandian, N. Siva Shanmugam, Investigations on mechanical properties and microstructural examination of activated TIG-welded nuclear-grade stainless steel, J. Braz. Soc. Mech. Sci. Eng., 42 (**2020**), 292, doi:10.1007/s40430-020-02393-4

[5] S. Celik, I. Ersozlu, Investigation of the mechanical properties and microstructure of friction welded joints between AISI 4140 and AISI 1050 steel, Mater. Des., 30 (**2009**) 4, 970–976, doi:10.1016/j.matdes.2008.06.070.

[6] M. N. Ahmad Fauzi, M. B. Uday, H. Zuhailawati, A. B. Ismail, Microstructure and mechanical properties of alumina-6061 aluminum alloy joined by friction welding, Mater. Des., 31 (**2010**) 2, 670–676, doi:10.1016/j.matdes.2009.08.019

[7] J. Luo, X. Wang, D. Liu, F. Li, J. Xiang, Inertia radial friction welding joint of large size H90 brass/D60 steel dissimilar metals, Mater. Manuf. Process., 27 (**2012**) 9, 930–935, doi:10.1080/10426914.2011.610087

[8] Z. W. Huang, H. Y. Li, G. Baxter, S. Bray, P. Bowen, Electron microscopy characterization of the weld line zones of inertia friction welded superalloy, J. Mater. Process. Technol., 211 (**2011**) 12, 1927–1936, doi:10.1016/j.jmatprotec.2011.06.019

[9] H. Seli, A. I. M. Ismail, E. Rachman, Z. A. Ahmad, Mechanical evaluation and thermal modeling of friction welding of mild steel and aluminium, J. Mater. Process. Technol., 210 (**2010**) 9, 1209–1216, doi:10.1016/j.jmatprotec.2010.03.007

[10] M. Kimura, K. Suzuki, M. Kusaka, K. Kaizu, Effect of friction welding condition on joining phenomena, tensile strength, and bend ductility of friction welded joint between pure aluminium and AISI 304 stainless steel, Journal of Manufacturing Processes, 25 (**2017**) 116–125, doi:10.1016/j.jmapro.2016.12.001

[11] M. Kimura, K. Suzuki, M. Kusaka, K. Kaizu, Effect of friction welding condition on joining phenomena and mechanical properties of friction welded joint between 6063 aluminium alloy and AISI 304 stainless steel, Journal of Manufacturing Processes, 26 (**2017**) 178–187, doi:10.1016/j.jmapro.2017.02.008

[12] G. Senthilkumar, R. Ramakrishnan, Design of Optimal Parameter for Solid-State Welding of EN 10028-P355 GH Steel Using Gray Incidence Reinforced Response Surface Methodology, Arabian Journal for Science and Engineering, 46 (**2021**) (3), 2613–2628, doi:10.1007/s13369-020-05169-z

[13] G. Senthilkumar, T. Mayavan, R. Ramakrishnan, Optimization for Friction Welding Input Factors to Maximize Tensile Strength and Minimize Axial Shortening in ASTM A516 Grade 70 Steel Rods, Journal of Applied Science and Engineering, 25 (**2021**) 5, 773–784, doi:10.6180/jase.202210_25(5).0008

[14] D. S. Correia, C. V. Goncalves, S. S. Cunha, V. A. Ferraresi, Comparison between genetic algorithms and response surface methodology in GMAW welding optimization, J. Mater. Process. Technol., 160 (**2005**) 1, 70–76, doi:10.1016/j.jmatprotec.2004.04.243

[15] P. M. Ajith, T. M. Afsal Husain, P. Sathiya, S. Aravindan, Multi-objective optimization of continuous drive friction welding process parameters using response surface methodology with the intelligent optimization algorithm, J. Iron Steel Res. Int., 22 (**2015**), 954–960, doi:10.1016/S1006-706X(15)30096-0

[16] M. Santhanakumar, R. Adalarasan, S. Siddharth, A. Velayudham, An investigation on surface finish and flank wear in hard machining of solution treated and aged 18% Ni maraging steel, J. Braz. Soc. Mech. Sci. Eng., 39 (**2017**), 2071–2084, doi:10.1007/s40430-016-0572-0

[17] R. Kadaganchi, M. R. Gankidi, H. Gokhale, Optimization of process parameters of aluminum alloy AA 2014–T6 friction stir welds by response surface methodology, Def. Technol., 11 (**2015**) 3, 209–219, doi:10.1016/j.dt.2015.03.003

[18] T. Atcharawadi, C. Boonruang, Design of boiler welding for improvement of lifetime and cost control, Materials, 9 (**2016**) 11, 891–906, doi:10.3390/ma9110891

[19] R. Selvaraj, K. Shanmugam, P. Selvaraj, B. Prasanna Nagasai, V. Balasubramanian, Optimization of Process Parameters of Rotary Friction Welding of Low Alloy Steel Tubes Using Response Surface Methodology, Forces in Mechanics, (**2023**) 100175, doi:10.1016/j.finmec.2023.100175

[20] G. Senthilkumar, R. Ramakrishnan, A study of individual and interaction effect of process parameters on friction welded AISI 410 and AISI 430 Joint, Materials Today Proceedings, 46 (**2021**) 9, 3233–3239, doi:10.1016/j.matpr.2020.11.206

[21] Banerjee Amborish, Michail Ntovas, Laurie Da Silva, Salaheddin Rahimi, Microstructure and mechanical properties of dissimilar inertia friction welded 316L stainless steel to A516 ferritic steel for potential applications in nuclear reactors, Manufacturing Letters, 33 (**2022**), 33-37, doi:10.1016/j.mfglet.2022.07.002

[22] Zhang Kejin, Xusheng Qian, Jieshi Chen, Junmei Chen, Hao Lu, Non-monotonic evolution of microstructure and fatigue properties of the round bar–plate rotary friction welding joints in 304 austenitic stainless steel, Materials & Design, 224 (**2022**), 111400, doi:10.1016/j.matdes.2022.111400

[23] R. Winiczenko, K. Mieczysław, Friction welding of ductile cast iron using interlayers, Materials & Design, 34 (**2012**), 444–451, doi:10.1016/j.matdes.2011.08.038

[24] P. Sathiya, S. Aravindan, A. Noorul Haq, Effect of friction welding parameters on mechanical and metallurgical properties of ferritic stainless steel, The International Journal of Advanced Manufacturing Technology, 31 (**2007**), 1076–1082, doi:10.1007/s00170-005-0285-5